Optical forces and optical torques on various materials arising from optical lattices in the Lorentz-Mie regime

Lin Jia[1] and Edwin L. Thomas[2,*]

[1]*Institute for Soldier Nanotechnologies, Department of Materials Science and Engineering, Massachusetts Institute of Technology, Cambridge, Massachusetts 02139, USA*

[2]*Dean of Engineering, Rice University, P.O. Box 1892, Houston, Texas 77251, USA*

(Received 10 April 2011; revised manuscript received 22 June 2011; published 16 September 2011)

By combining the Maxwell stress tensor with the finite-difference time-domain (FDTD) method, we calculate the optical force and optical torque on particles from optical lattices. We compare our method to the two-component method and the electrostatic approximation (ESA). We also discuss how particle's refractive index, shape, size, and the morphology of an optical lattice influence optical forces and the condition to form stable optical trapping wells. In addition to optical forces, optical torque from one dimensional (1D) optical lattice is discussed for particles having anisotropic shapes; metastable and stable equilibrium orientation states are found. A detailed understanding of the optical force and torque from optical lattices has significant implications for optical trapping, micromanipulation, and sorting of particles.

DOI: 10.1103/PhysRevB.84.125128 PACS number(s): 78.67.Bf, 87.80.Cc, 07.05.Tp, 78.20.Bh

I. INTRODUCTION

The interaction of electromagnetic (EM) waves and materials leads to the reflection, refraction, and absorption of EM waves. Since the momentum of the EM waves is changed during the process, the EM waves exert forces on the materials to keep the total momentum conserved, as was first pointed out by Maxwell in 1873.[1] The application of optical forces was first explored by Ashkin using a highly focused laser beam to trap micro-objects. This breakthrough was later termed "optical tweezers" or "optical traps."[2–5] Since then, various forms of optical fields have been developed to achieve optical micromanipulation and optical sorting, including optical vortex,[6,7] holographic optical tweezers,[8,9–14] interferometric optical tweezers,[15–20] standing wave,[21–26] plasmonic resonances,[27–32] and optical lattices.[33–37] The rapid development of optical micromanipulation provides many applications in various fields, including sorting of cells, macromolecules, and colloids,[24,36,38–46] colloidal crystals evolution,[33–35,47] nanofabrication,[9] quantum simulation,[8] micro- and nanomotors,[48,49] and the study of the physical properties of biology systems including DNA at the molecular level.[50–57]

The numerical calculations of optical forces are clearly very important to support, design, and nurture the continued fast development of the experiments and the industrial applications of optical micromanipulation, trapping, and sorting. This fact has led to the development of multiple numerical techniques including (1) generalized Lorenz-Mie theory,[58] which is suitable for calculating optical forces on objects of particular shapes including spherical, spheroid, and cylinder shapes;[58–60] (2) the gradient-force intuitive approach,[61] which is suitable for a strongly focused light source; (3) the T-matrix method,[62,63] which is suitable for highly symmetric systems; (4) the discrete dipole approximation,[64] which needs to satisfy two validation criteria and is computationally cumbersome;[64] and (5) the electrostatic approximation (ESA) method,[23,65] which calculates the optical forces on particles with refractive index close to the background medium. Recently, finite-difference time-domain (FDTD) was also used to calculate the optical force and the acoustic force on micro- and nanoparticles,[66–72] but this method has not been extended to optical-lattice applications.

In this paper we combine a previously reported 3D-FDTD simulation[72,73] and the Maxwell stress tensor ($\tilde{\mathbf{T}}$) to compute both optical forces and optical torques from optical lattices on particles in the Lorentz-Mie regime. The computation method is versatile: It can be applied to calculate optical forces and torques on objects of arbitrary shape and does not require system symmetry. The calculation covers the Lorentz-Mie regime (object size $\approx$ wavelength) where most applications of optical trapping, micromanipulation, and sorting reside. The method can be applied to both dielectric and absorbing objects. The two-component method[74] and the ESA method[23,65] were previously used to calculate optical forces from optical lattices. In contrast the method employed here is still effective even if the refractive-index contrast between the particle and the background is high.

The approach can calculate optical forces and optical torques from various forms of optical fields; we specifically focus on optical lattices in this paper. Compared to other techniques, optical trapping and sorting using optical lattices have two advantages. (1) The number of trapping sites is high, up to hundreds; the trapping sites are periodic and can exhibit various optical intensity morphologies.[75] (2) The optical sorting area is large, and control can be automated to offer high throughput sorting. These advantages enable interesting applications. For example, optical lattices can assemble particles to make optical matter including photonic and phononic crystals[34] or potentially even dual-band gap crystals.[76,77] Recently optical lattices have been extended to a quasicrystalline substrate potential, which assembles particles to the Archimedean-like tiling.[35] In addition to micromanipulations optical lattices can also be used to achieve passive, parallel, and high-throughput optical sorting.[36,37] Furthermore the optical-mechanical coupling is observed in optical lattices: the optical-binding effect[33,78] leads to collective oscillations[79]

and spatially localized vibration with multiple modes in optical matter.[80]

II. NUMERICAL APPROACH

According to the momentum conservation theorem, the force on an object at a specific time can be calculated by

$$f = \int_{\partial S_0} \tilde{\mathbf{T}} \cdot \mathbf{n}\, dS - \partial \left[\int_V \mathbf{D}(\mathbf{r},t) \times \mathbf{B}(\mathbf{r},t) dV \right] \Big/ \partial t. \quad (1)$$

Here ∂S_0 is a closed surface over the object and $\mathbf{n}$ is the surface-normal vector. $\tilde{\mathbf{T}}$ is the Maxwell stress tensor expressed as

$$T_{i,j} = D_i E_j + B_i H_j - (\mathbf{E}\cdot\mathbf{D} + \mathbf{B}\cdot\mathbf{H})\delta_{i,j}/2. \quad (2)$$

Here we used Minkowski formulation, which has been proved to be accurate by comparison with bound charges/currents approach.[81–83] Further, the Maxwell stress tensor in Eq. (2) can be directly deduced by comparing Lorentz force and the mechanical force expressed in Eq. (1).[81–83] The Maxwell stress tensor is calculated by a FDTD simulation. Equation (1) is then used to calculate optical forces.[72] We assume that EM waves are time-harmonic fields. The time-averaged value of $\partial[\int_V \mathbf{D}(\mathbf{r},t) \times \mathbf{B}(\mathbf{r},t) dV]/\partial t$ is zero; therefore, the time-averaged force is

$$\mathbf{F} = \frac{1}{\tau} \int_0^\tau dt \int_{\partial S_0} \tilde{\mathbf{T}} \cdot \mathbf{n}\, dS. \quad (3)$$

Here τ is the period of the light source. In addition to the net force the torque can be calculated by

$$\Omega = -\frac{1}{\tau} \int_0^\tau dt \int_{\partial S_0} \mathbf{n} \cdot \tilde{\mathbf{T}} \times \mathbf{r} dS. \quad (4)$$

Here $\mathbf{r}$ is the vector from the center of mass of the object to the surface element ∂S_0.

III. RESULTS AND DISCUSSIONS

In our numerical calculation the wavelength of the light source in vacuum (λ) is fixed at 1064 nm to relate to the wavelength of the widely used solid-state lasers (Nd: YAG and Nd: YLF). All calculation results are applicable to other typical wavelengths via scaling along with incorporation of the dispersion of the refractive index. We first consider the simplest case of a one-dimensional (1D) periodic optical lattice arising from the interference of two plane waves propagating along opposite directions in a uniform lossless medium. We assume that the medium is water and the refractive index n_m is taken as 1.3. The light intensity is calculated by

$$I = \frac{1}{\tau} \int_0^\tau \left(\sum_{i=1}^N \mathbf{E}_i \right) \cdot \left(\sum_{i=1}^N \mathbf{E}_i \right) dt, \quad (5)$$

where N is the number of plane waves. The electronic component of the first plane wave is given by $\mathbf{E}_1 = E_0 \exp(ik_0 y - i\omega t)\hat{z}$, and the electronic vector of the second plane wave is $\mathbf{E}_2 = E_0 \exp(-ik_0 y - i\omega t)\hat{z}$; here $k_0 = 2\pi n_m/\lambda$ and the polarization of the two plane waves is along $\hat{z}$ direction. From Eq. (5) the light intensity is

$$I = E_0^2 + E_0^2 \cos(2k_0 y). \quad (6)$$

From Eq. (6) the period of the optical lattice (l) is 409 nm. We next introduce a dielectric sphere with diameter d. The refractive index of the particle (n_s) is taken as 1.58 ($n_s/n_m = 1.2$), which is typical for polystyrene spheres. We are interested in particles that have size that is comparable to the period of the optical lattice. Specifically, we focus on three kinds of particles: 120-nm diameter ($d/l = 0.293$), 300-nm diameter ($d/l = 0.733$), and 540-nm diameter ($d/l = 1.32$). We change the positions of the centers of the particles (y) in the optical lattices and calculate the optical forces. From Eqs. (1)–(4) optical forces are directly proportional to the light source power, thus we express the force in the form of F/E_0^2. The results are shown as the solid lines in Figs. 1(a), 1(b), and 1(c), and the dashed lines are the light intensity distribution. In Figs. 1(a) and 1(b) the optical forces push the sphere center to the high light-intensity positions and trap it there. In Fig. 1(c), however, optical forces push the center of the sphere to the lowest light-intensity positions. From Figs. 1(a), 1(b), and 1(c), we find that the optical force can be expressed as

$$F(x,y,z) = F_0 C(x,y,z), \quad (7)$$

where $C(x,y,z)$ is a function of the particle position in the optical lattice and indicates how the optical force changes with the particle position. In the 1D-optical lattices $C(x,y,z)$ is only related to y because of the system symmetry, thus it can be expressed as $C(y)$. Comparing $C(y)$ in Figs. 1(a), 1(b), and 1(c) demonstrates a perfect match, which is shown in Fig. 1(d).

The maximum force the particle experiences is F_0, and it is a function of the particle size and permittivity. We assume that F_0 is negative when optical forces push the particle center to the low light-intensity positions. Figure 2 shows how F_0 changes with the diameter of the particle d. F_0 increases with particle diameter until the diameter is around the period of the optical lattice, and then F_0 drops quickly with increasing diameter and becomes negative in some range.

We can understand how the optical forces on particles arise from optical lattices from examining the energy aspect. We first assume that the dielectric particle can be modeled as a set of multiple dipoles. The interaction energy between a single dipole $\mathbf{p}$ and the electric field $\mathbf{E}$ is $-\mathbf{p}\cdot\mathbf{E}$. If the refractive index of the particle is near to the background material, $\mathbf{p}$ and $\mathbf{E}$ are generally in phase, so the particles are pushed into high light-intensity positions to achieve minimum interaction energy. When the diameter of the particle is smaller than the period of the optical lattice, the optical forces push the particle center to the high light-intensity positions and the particle stabilizes at the light-intensity peaks. However, if the diameter of the particle is bigger than the period, the particle can span two light-intensity peaks within the particle when its center lies in the low light-intensity positions. As the diameter increases continually, the particle center may return to high light-intensity positions to hold three peaks in the material, so F_0 oscillates as d increases. Figure 2 shows the oscillation of F_0 in the range of 6 nm $< d <$ 540 nm ($0.015 < d/l < 1.320$). To quantitatively explain Fig. 2, we define the following parameter to represent how much of the EM field is inside the particle:

$$\sigma = -\iiint_{V_0} I(x,y,z) dx dy dz. \quad (8)$$

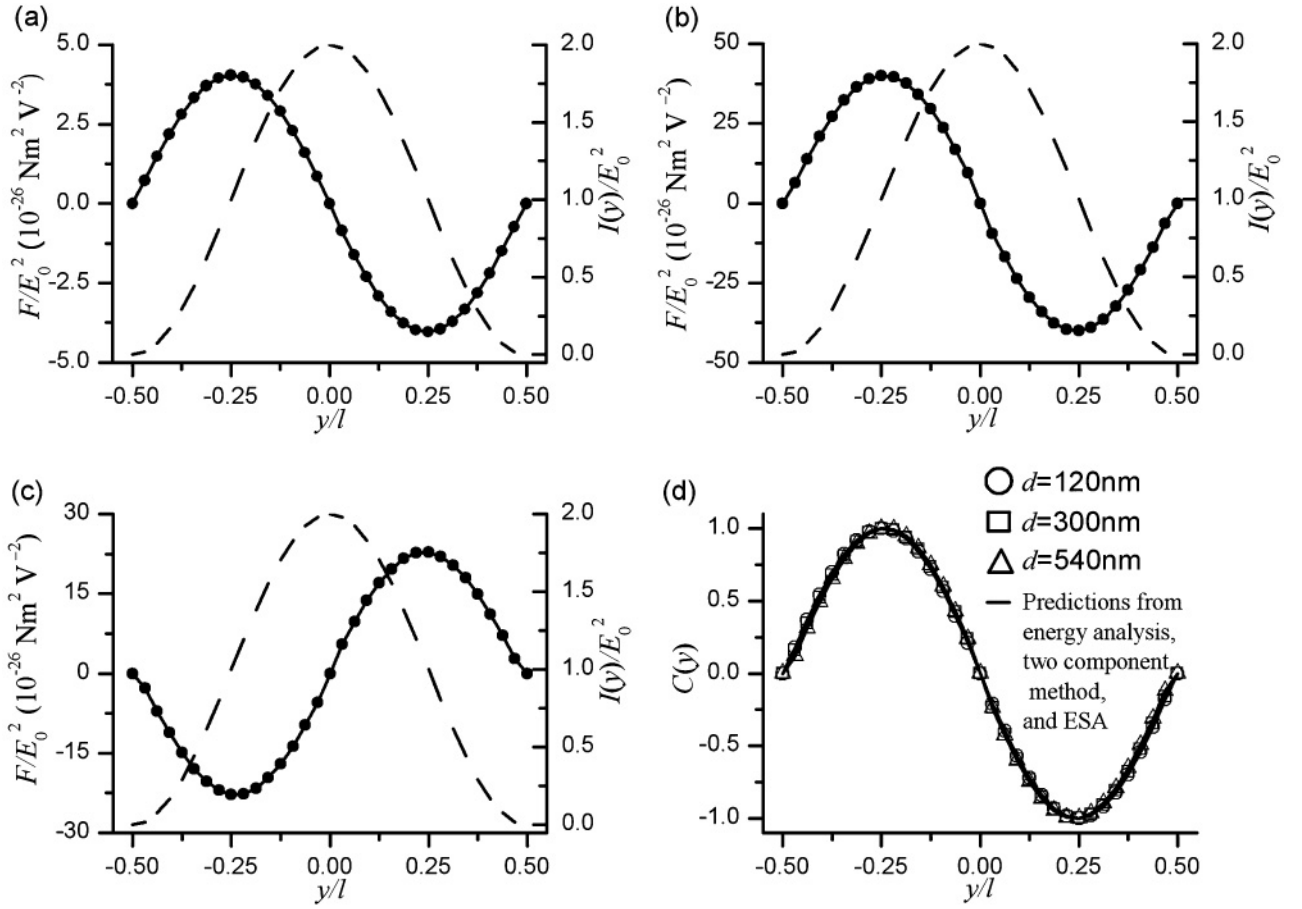

FIG. 1. Optical forces for particles with (a) 120-nm diameter, (b) 300-nm diameter, (c) 540-nm diameter. (d) The trends for optical forces acting on particles of different sizes agree with the theoretical predictions.

Here V_0 is the region occupied by the particle and $I(x,y,z)$ is the light intensity of the optical lattice. The parameter σ represents the interaction energy between the particle and the optical lattice, thus the optical force should be directly proportional to the spatial derivative of the parameter σ:

$$F \propto -\nabla\sigma = \iiint_{V_0} \nabla I(x,y,z)dV. \quad (9)$$

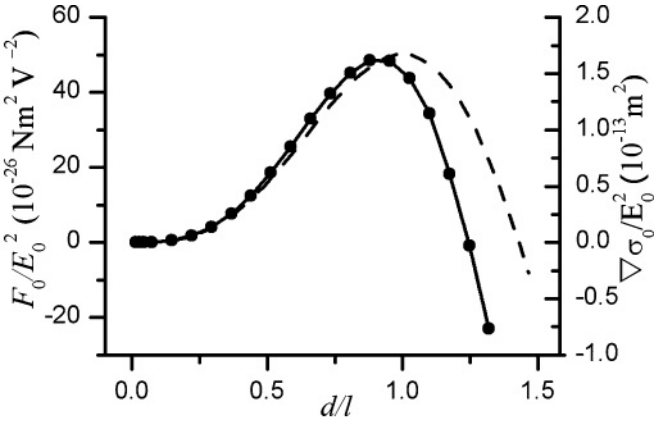

FIG. 2. F_0 in the range of $0 < d < 1.5l$. The broken line is $\nabla\sigma_0/E_0^2$.

For the 1D-optical lattice, the maximum optical force is

$$F_0 = -\nabla\sigma_0 \approx 2E_0^2 k_0 \iiint_{V_0} \sin\left[2k_0(y+0.25l)\right]dV. \quad (10)$$

In Eq. (10) the particle center is at the origin of the coordinates. We plot $\nabla\sigma_0/E_0^2$ as the dotted line in Fig. 2. The reason for the shape differences between $\nabla\sigma_0/E_0^2$ and F_0/E_0^2 is that the light intensity in Eq. (8) is calculated from light intensity of the optical lattice; the actual field inside the particle is different from the field of the optical lattice. Despite this, $\nabla\sigma_0/E_0^2$ gives a very good approximation to F_0 in the range of $0 < d < l$.

Except for the energy aspect, optical forces from optical lattices can also be calculated by the two-component method.[74] The trapping abilities of optical lattices mainly come from gradient force. The particle can be assumed as a set of dipoles. For a single dipole its polarization is proportional to the electric field applied on it and can be expressed by Clausius-Mossotti relation:

$$\mathbf{P}(\mathbf{r},t) = 3\varepsilon_m\varepsilon_0(\varepsilon_s - \varepsilon_m)/(\varepsilon_s + 2\varepsilon_m)\mathbf{E}_{\text{applied}}(\mathbf{r},t). \quad (11)$$

By employing (11), the gradient force on the dipole can be expressed as

$$\mathbf{f}_{\text{grad}}(\mathbf{r},t) = 3\varepsilon_0\varepsilon_m(\varepsilon_s - \varepsilon_m)/(2\varepsilon_s + 4\varepsilon_m)\nabla\mathbf{E}^2_{\text{applied}}(\mathbf{r},t)dV. \quad (12)$$

Here dV is the volume of the dipole. The total force on the particle is the integral of Eq. (12) over the volume of particle, thus

$$\mathbf{F}_{\text{grad}}(\mathbf{r}) = 3\varepsilon_m\varepsilon_0(\varepsilon_s - \varepsilon_m)/(2\varepsilon_s + 4\varepsilon_m) \times \iiint_{V_0} \nabla\left\langle \boldsymbol{E}^2_{\text{applied}}(\mathbf{r},t)\right\rangle_\tau dV. \quad (13)$$

In Eqs. (11)–(13) the applied field $E_{\text{applied}}(r,t)$ on the dipole contains both the electric field from other dipoles and the electric field of the light source. If the particle is small and the refractive index of the particle is near to the background, the impact from other dipoles can be omitted, thus

$$\mathbf{F}_{\text{grad}}(\mathbf{x},\mathbf{y},\mathbf{z}) \approx 3\varepsilon_m\varepsilon_0(\varepsilon_s - \varepsilon_m)/(2\varepsilon_s + 4\varepsilon_m) \times \iiint_{V_0} \nabla I(x,y,z)dV. \quad (14)$$

The ESA method is also used to calculate optical forces from optical lattices.[23,65] The energy difference caused by introducing particles into optical lattices can be expressed by

$$\Delta W = \iiint_V (\mathbf{ED} - \mathbf{E}_i\mathbf{D}_i + \mathbf{HB} - \mathbf{H}_i\mathbf{B}_i)/2dV. \quad (15)$$

Here V is the volume of the whole system; $\mathbf{E},\mathbf{D},\mathbf{B},\mathbf{H}$ are the fields after the particle is introduced into the optical lattice; and $\mathbf{E}_i,\mathbf{D}_i,\mathbf{B}_i,\mathbf{H}_i$ are the fields before the particle is introduced. Equation (15) can be transformed into

$$\Delta W = -\varepsilon_0\varepsilon_m(\varepsilon_s/\varepsilon_m - 1)/2 \iiint_{V_0} \mathbf{E}\mathbf{E}_i dV. \quad (16)$$

Here V_0 is the volume of the particle. From Eq. (16),

$$\mathbf{F}_{\text{grad}}(\mathbf{r}) = -\langle\nabla(\Delta W)\rangle_\tau = \varepsilon_0\varepsilon_m(\varepsilon_s/\varepsilon_m - 1)/2 \times \iiint_{V_0} \nabla(\langle\mathbf{E}\mathbf{E}_\mathbf{i}\rangle_\tau)dV. \quad (17)$$

The expression in Eq. (17) is not explicit because it needs information of the optical field inside the particle. $\mathbf{E}$ should be the sum of $\mathbf{E}_i$ and the electric field from the material polarization. If the refractive index of the particle is near to the background and the particle size is small, the material polarization is omitted and $\mathbf{E}_i$ is used to replace $\mathbf{E}$, which leads to

$$\mathbf{F}_{\text{grad}}(x,y,z) = \varepsilon_0\varepsilon_m(\varepsilon_s/\varepsilon_m - 1)/2 \iiint_{V_0} \nabla I(x,y,z)dV. \quad (18)$$

The two-component method is a higher order approximation for calculating optical forces compared to the ESA method because the Clausius-Mossotti relation in the two-component method gives an approximation to the electric field from the material polarization. Equation (14) can be deduced from Eq. (17): if the particle size is small compared to wavelength, the following equation is effective:

$$\mathbf{E} = 3\mathbf{E}_i\varepsilon_m/(\varepsilon_s + 2\varepsilon_m). \quad (19)$$

Inserting Eq. (19) into Eq. (17) leads to Eq. (14).

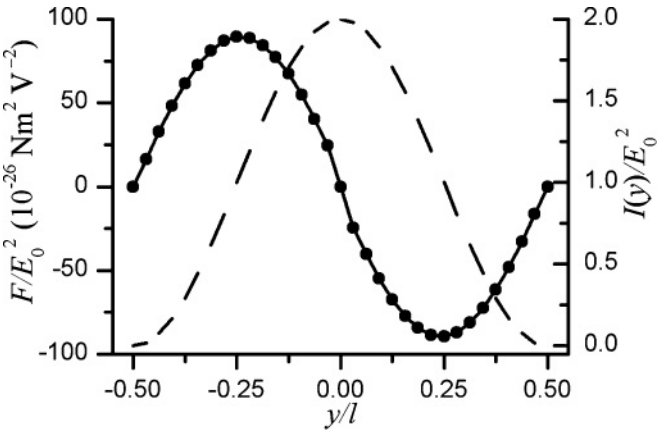

FIG. 3. Optical forces for titanium particle of 300-nm diameter.

No matter what method is used to understand the optical forces from optical lattices, the forms of optical forces in Eqs. (9), (14), and (18) are similar. Thus Eq. (7) can be expressed as

$$F = \varepsilon_0\eta(n_m,n_s) \iiint_{V_0} \nabla I(x,y,z)dV. \quad (20)$$

In Eq. (20) the impact of the optical-lattice morphology, the particle shape, and size on optical forces is represented in the volume integral $\iiint_{V_0} \nabla I(x,y,z)dV$. We calculate the volume integral to determine how the optical force changes for particles at different positions and plot it as a solid line in Fig. 1(d). Comparison of the FDTD simulation results with the predictions from physical theory shows an excellent match. Optical force is also impacted by refractive index of the particle. We next calculate the optical force on a titanium particle of 300-nm diameter (dielectric, $n_s = 2.7$ and $n_s/n_m = 2.08$), which is shown in Fig. 3. The shape of optical force line in Fig. 3 is very similar to Fig. 1, and the amplitude of the optical force increases. The impact of refractive index is represented in the parameter $\eta(n_m,n_s)$ in Eq. (20). From the two-component method $\eta(n_m,n_s) = 3n_m^2(n_s^2 - n_m^2)/(2n_s^2 + 4n_m^2)$; from the ESA method $\eta(n_m,n_s) = 0.5(n_s^2 - n_m^2)$.

We next compare parameter $\eta(n_m,n_s)$ from our FDTD simulation, the two-component method,[74] and the ESA method;[23,65] the results are shown in Fig. 4. Results from the two-component method and the ESA method match the FDTD calculation very well in the low refractive-index range. They are suitable for low relative refractive-index situations; thus, they deviate from FDTD calculation at high index contrast ($n_s/n_m > 1.7$).

From Fig. 4 optical forces increase as the refractive-index contrast increases, and then they decrease. If we assume the particle as a set of dipoles, the electric field experienced by dipole N consists of electric fields of the light source and all the other dipoles:

$$\mathbf{E}_{\text{applied},N} = \mathbf{E}_{ol,N} + \sum_M \mathbf{E}_{NM}. \quad (21)$$

Here $\mathbf{E}_{ol,N}$ is the electric field of the optical lattice at the position of dipole N. $\mathbf{E}_{NM}$ is the electric field of dipole M at

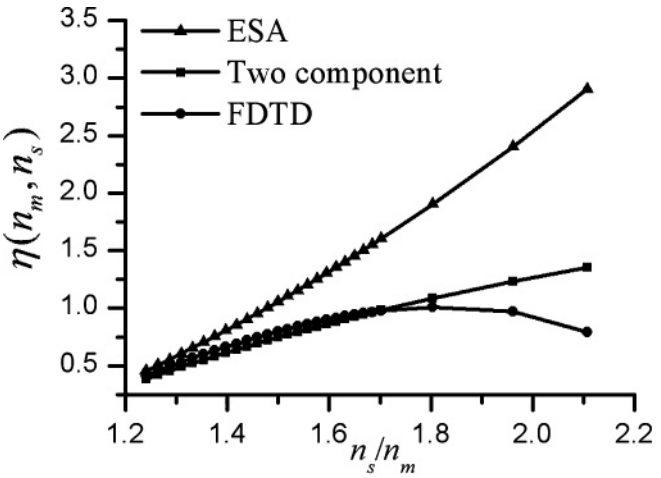

FIG. 4. Parameter $\eta(n_m,n_s)$ calculated by FDTD simulation, the two-component method, and the ESA method.

the position of dipole N, and it is given by

$$\mathbf{E}_{NM} = \exp(ikr_{NM})\left[\left(k^2/r_{NM} + ik/r_{NM}^2 - 1/r_{NM}^3\right)\mathbf{p}_M + \left(-k^2/r_{NM} - 3ik/r_{NM}^2 + 3/r_{NM}^3\right)\hat{\mathbf{r}}_{NM}(\hat{\mathbf{r}}_{NM}\cdot\mathbf{p}_M)\right], \tag{22}$$

where r_{NM} is the distance between dipole M and dipole N. The dipole moment of dipole N is

$$\mathbf{p}_N = \alpha\left(\mathbf{E}_{ol,N} + \sum_M \mathbf{E}_{NM}\right). \tag{23}$$

Here $\alpha = 3\varepsilon_m\varepsilon_0(\varepsilon_s - \varepsilon_m)/(\varepsilon_s + 2\varepsilon_m)V_d$ and V_d is the volume of the dipole.

From Eqs. (22) and (23) we have

$$\sum_M A_{NM}\mathbf{p}_M = \alpha\mathbf{E}_{ol,N}. \tag{24}$$

Every dipole generates an equation such as Eq. (24). In the matrix A every component is a polynomial function of α. If we solve the set of equations, the final solution has the form

$$\mathbf{p}_M = Z_{M,1}(\alpha). \tag{25}$$

Here $Z_{M,1}(\alpha)$ is a polynomial function of α. Inserting Eq. (25) into Eq. (22), we have

$$\mathbf{E}_{NM} = Z_{NM}(\alpha), \tag{26}$$

thus,

$$\mathbf{E}_{\text{applied},N} = \mathbf{E}_{ol,N} + \sum_M Z_{NM}(\alpha) = \mathbf{E}_{ol,N} + \sum_M Z_{NM} \times[3\varepsilon_0\varepsilon_m V_d(\varepsilon_s - \varepsilon_m)/(\varepsilon_s + 2\varepsilon_m)]. \tag{27}$$

Inserting Eq. (27) into Eq. (13), we find that optical force is a complex polynomial function of the refractive index of the particle. Optical forces initially increase as the refractive index of the particle increases; after refractive-index contrast exceeds some value (for 300-nm-spherical particles this value is 1.8), the optical forces fluctuate as the refractive index increases.

From Fig. 1 the optical force from the optical lattice is a restoring force, and trapping-potential wells form at the stable equilibrium positions. The shape of optical force lines in Fig. 1 is very near to a sinusoidal shape, thus the depth of the potential well is

$$U = \int_0^{0.5l} F_0 C(x,y,z)dy \approx \int_0^{0.5l} F_0 \sin(2\pi y/l)dy = F_0 l/\pi. \tag{28}$$

In real particle systems at finite temperatures Brownian movement causes positional fluctuation. The effect of Brownian movement on optical trapping can be calibrated by a factor m that depends on the relative strength of the potential versus the thermal energy,

$$m = U/kT. \tag{29}$$

It is assumed that the trapping force can overcome the effect of Brownian movement when $m > 10$.[2] From Eqs. (28) and (29):

$$m = U/kT \approx F_0 l/\pi kT = F_0 l Q/\pi kTc\varepsilon_0 n_m E_0^2. \tag{30}$$

Here Q represents the power of the optical lattice ($Q = c\varepsilon_0 n_m E_0^2$). If we assume that the power is $5mW/\mu m^2$ and $T = 300K$, inserting these values into Eq. (30) gives

$$m \approx F_0/E_0^2 \times 4.56 \times 10^{25}. \tag{31}$$

From Fig. 2 F_0/E_0^2 varies as d increases, therefore the trapping ability changes for particles of different sizes. For example, when the diameter is around the period of optical lattices, $m \approx 20$, the trapping force is sufficient to overcome the Brownian movement so particles mainly reside in the high light-intensity positions. For other particle sizes such as $d \approx 1.3l$, however, F_0/E_0^2 is nearly zero. The particles will wander among the optical lattice because of their dominant Brownian movement, and the trapping effect can be ignored. Our calculation method matches with the experimental result observed in Ref. 26.

Next, we consider a three-dimensional (3D) periodic optical lattice arising from the interference of six plane waves. Their electric fields are depicted by:

$$E_1 = E_0\exp(ik_0 y - i\omega t)\hat{z} \tag{32}$$

$$E_2 = E_0\exp(-ik_0 y - i\omega t)\hat{z} \tag{33}$$

$$E_3 = E_0\exp(ik_0 z - i\omega t)\hat{x} \tag{34}$$

$$E_4 = E_0\exp(-ik_0 z - i\omega t)\hat{x} \tag{35}$$

$$E_5 = E_0\exp(ik_0 x - i\omega t)\hat{y} \tag{36}$$

$$E_6 = E_0\exp(-ik_0 x - i\omega t)\hat{y} \tag{37}$$

Here $k_0 = 2\pi n_m/\lambda$, and the light intensity is

$$I(x,y,z) = 3E_0^2 + E_0^2\cos(2k_0 x) + E_0^2\cos(2k_0 y) + E_0^2\cos(2k_0 z). \tag{38}$$

The highest light-intensity positions are simple cubic lattice, and the period of the optical lattice (l) is 409 nm. Equation (38) is a simple approximation to the P-minimal surface having $Pm\bar{3}m$ symmetry.[84,85] From Eq. (38) the origin of the coordinate system is a high light-intensity position. We calculate the optical force on two kinds of spherical particles:

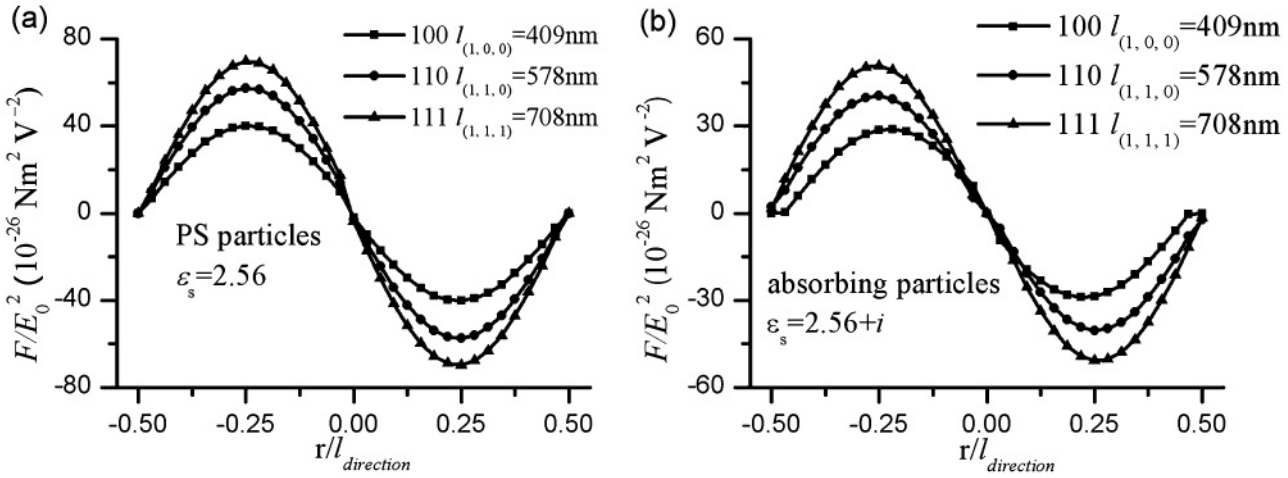

FIG. 5. (a) Optical forces on polystyrene particles arising from the 3D-optical lattice. The shapes of the optical-force lines along different directions are similar. The amplitudes of the optical forces fulfill $F_{\max[1,0,0]} = F_{\max[1,1,0]}/\sqrt{2} = F_{\max[1,1,1]}/\sqrt{3}$. (b) Optical forces on absorbing particles arising from the 3D-optical lattice.

polystyrene particle with permittivity 2.56 and absorbing particles with permittivity $2.56 + i$. The diameter of the particles is 300 nm. We change the positions of the centers of the particles $r = (x^2 + y^2 + z^2)^{0.5}$ along [100], [110], and [111] directions and calculate the optical forces. The results are shown in Fig. 5. In Fig. 5(a) optical forces along different directions fulfill $F_{\max[100]} = F_{\max[110]}/\sqrt{2} = F_{\max[111]}/\sqrt{3}$. This can be understood from Eq. (9): $\mathbf{F} \propto \nabla I(x,y,z)$. Inserting Eq. (38) into the Eq. (9) leads to

$$\mathbf{F} \propto \sin(2k_0x)\hat{x} + \sin(2k_0y)\hat{y} + \sin(2k_0z)\hat{z}. \tag{39}$$

From Eq. (39) the restoring force pushes the particle to high light-intensity positions, where optical potential wells form. The depth of the potential well is different along different directions and the shallowest potential is along the [100] direction. Compared to the 1D-optical lattice, the 3D-optical lattice offers 3D trapping; the depth of the potential well in 3D-optical lattice is similar to the 1D-optical lattice.

In addition to dielectric particles, optical trapping has been extended to absorbing particles.[86–89] The permittivity of absorbing particles has imaginary part $\varepsilon = \varepsilon_1 + i\varepsilon_2$. For Rayleigh particles the gradient optical force is

$$F = |\alpha|\,\nabla E^2/2. \tag{40}$$

In Eq. (40) α is the polarizability and can be expressed as

$$|\alpha| = 3V_{\text{eff}}|(\varepsilon_1 + i\varepsilon_2 - \varepsilon_m)/(\varepsilon_1 + i\varepsilon_2 + 2\varepsilon_m)|. \tag{41}$$

In Eq. (41) the effective volume (V_{eff}) is smaller than the space volume of the particle because of the absorption:[88]

$$V_{\text{eff}} = 4\pi \int_0^{0.5d} r^2 \exp[-(0.5d - r)/\delta]dr, \tag{42}$$

where δ is the skin depth and can be calculated from the permittivity of the particle,

$$\delta = \lambda/2\pi\sqrt{\left(\sqrt{\varepsilon_1^2 + \varepsilon_2^2} - \varepsilon_1\right)/2}. \tag{43}$$

From Eqs. (40) and (41) the effect of absorption on optical force is determined by the effect of absorption on polarizability:

$$\begin{aligned} F_{\varepsilon=\varepsilon_1}/F_{\varepsilon=\varepsilon_1+i\varepsilon_2} &= |\alpha|_{\varepsilon=\varepsilon_1}/|\alpha|_{\varepsilon=\varepsilon_1+i\varepsilon_2} \\ &= [V\,|(\varepsilon_1 - \varepsilon_m)/(\varepsilon_1 + 2\varepsilon_m)|] \\ &\quad /[V_{\text{eff}}|(\varepsilon_1 + i\varepsilon_2 - \varepsilon_m)/(\varepsilon_1 + i\varepsilon_2 + 2\varepsilon_m)|]. \end{aligned} \tag{44}$$

The permittivity absorption part ε_2 increases $|(\varepsilon_1 + i\varepsilon_2 - \varepsilon_m)/(\varepsilon_1 + i\varepsilon_2 + 2\varepsilon_m)|$ and decreases $V_{\text{eff}} = 4\pi \int_0^{0.5d} r^2 \exp[-(d/2 - r)/\delta]dr$. For absorbing particles in Lorenz-Mie range, however, the size of particles is usually higher than the skin depth, and the electric field inside the particle gets smaller because of the absorption. According to Eq. (17) absorption generally leads to smaller optical force. This is confirmed by comparing Figs. 5(a) and 5(b): absorption causes optical forces to decrease by 25%.

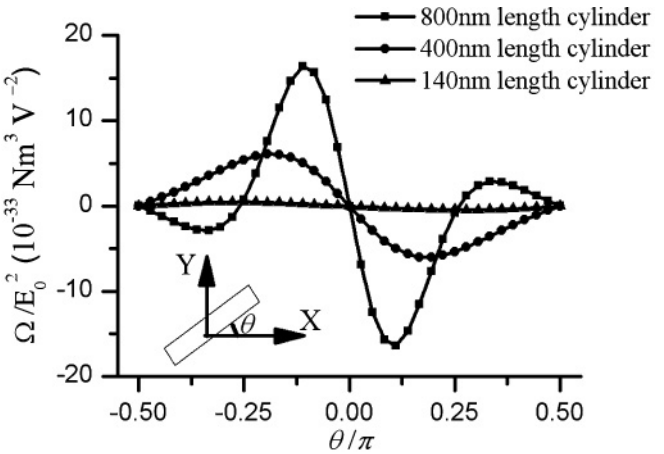

FIG. 6. Optical torques on three kinds of cylinders. For the 140-nm-length cylinder, we have not observed stable equilibrium orientations. For the 400-nm-length cylinder, $\theta = 0$ is the stable equilibrium orientation. For the 800-nm-length cylinder, in addition to the stable equilibrium orientation at $\theta = 0$, metastable orientation is observed at $\theta = \pm 0.5\pi$.

Our previous discussions concern spherical particles; to date, nonspherical micro- and nanostructures have been fabricated in experiments through multiple methods such as holographic interference lithography,[90] stop-flow interference lithography,[91] and the modification and aggregation of spherical particles.[92,93] In addition to optical forces optical lattices also apply optical torques on these nonspherical structures, offering the possibility to simultaneously control the position and orientation of particles. We now calculate the optical torque on particles in the 1D-optical lattices discussed previously. Three forms of particles are examined: a cylinder with 140-nm length and 140-nm diameter (aspect ratio 1), a cylinder with 400-nm length and 80-nm diameter (aspect ratio 5), and a cylinder with 800-nm length and 60-nm diameter (aspect ratio 13.3); the particles have near-identical volumes. We fix their centers at the highest light-intensity positions, and the particles rotate in XY plane. As shown in Fig. 6, the angle between the long axis of the particle and X axis is defined as θ. The optical torques on the cylinders as a function of angle of the cylinder axis (θ) are shown in Fig. 6, which shows that optical torques on particles of various shapes are very different. Optical torques on particles can also be understood from the aspect of energy. The interaction energy between a dielectric particle and optical lattice is expressed in Eq. (16), thus

$$\Omega = -\partial(\Delta W)/\partial\theta = \varepsilon_0\varepsilon_m(\varepsilon_s/\varepsilon_m - 1)/2 \times\partial\left(\iiint_{V_0}\mathbf{E}\mathbf{E}_i dV\right)\Big/\partial\theta. \quad (45)$$

From (45) the physical origin of optical torque is that the particle adopts particular orientations to minimize the interaction energy. If the refractive index of particles is near to the background (e.g., polystyrene, silica particles in distilled water), we can assume $\mathbf{E} = 6\varepsilon_m\mathbf{E}_i/(2\varepsilon_s + 4\varepsilon_m)$; this leads to

$$\Omega = 3\varepsilon_0\varepsilon_m(\varepsilon_s - \varepsilon_m)/(2\varepsilon_s + 4\varepsilon_m)\partial\left(\iiint_{V_0} I(x,y,z)dV\right)/\partial\theta. \quad (46)$$

For particles with near spherical shape or with a size much smaller than the period of optical lattices, optical torques on them are small because the total light intensity inside does not change much as the particles rotate with respect to the optical lattice $\partial(\iiint_{V_0} I(x,y,z)dV)/\partial\theta \approx 0$. Figure 6 confirms that the 140-nm length cylinder has a size much smaller than the period of the optical lattice (409 nm), and its shape is near-to-spherical compared to other cylinders calculated; thus, the optical torque on it is nearly zero compared to other cylinders. For particles with large aspect ratio and sizes comparable to the period of optical lattices, $\theta = 0$ is the stable equilibrium state. For the cylinder with aspect ratio 13.3, however, the two ends of the cylinder are both in at high intensity regimes at $\theta = 0.5\pi$, so in addition to the stable equilibrium state of $\theta = 0$, a metastable state of $\theta = 0.5\pi$ exists.

IV. CONCLUSION

In summary the optical force and optical torque from optical lattices are important for a wide variety of physical phenomena, ranging from optical trapping, optical micromanipulation, and optical sorting. The optical force is a function of optical lattice morphology and the refractive index, size, shape, and orientation of the particle. Optical force can be expressed as $F = \varepsilon_0\eta(n_m,n_s)\iiint_{V_0}\nabla I(x,y,z)dV$: the parameter $\eta(n_m,n_s)$ increases with the particle-refractive index up to $n_m/n_s = 1.8$, then it fluctuates as n_m increases. Absorption generally leads to smaller optical forces in the Lorentz-Mie regime. In the range of $0 < d < 1.5l$ the optical force reaches the maximum when the size of particle is around the period of the optical lattice. For particles near to spherical shape or with a size much smaller than the period of the optical lattice, optical torque is small compared to particles with size comparable to the period of the optical lattice and large aspect ratio. Both metastable and stable equilibrium orientation states exist for cylinder particles in the 1D-optical lattice.

ACKNOWLEDGMENTS

This research was supported by the US Army Research office through the Institute for Soldier Nanotechnologies under Contract W911NF-07-D-0004. We thank Dr. Jae-Hwang Lee for helpful discussions.

*Corresponding author: elt@rice.edu.

[1] J. C. Maxwell, *A Treatise on Electricity and Magnetism* (Oxford, 1873).
[2] A. Ashkin, J. M. Dziedzic, J. E. Bjorkholm, and S. Chu, Opt. Lett. **11**, 288 (1986).
[3] A. Ashkin and J. M. Dziedzic, Science **235**, 1517 (1987).
[4] A. Ashkin, J. M. Dziedzic, and T. Yamane, Nature **330**, 769 (1987).
[5] K. C. Neuman and S. M. Block, Rev. Sci. Instrum. **75**, 2787 (2004).
[6] L. Paterson, M. P. MacDonald, J. Arlt, W. Sibbett, P. E. Bryant, and K. Dholakia, Science **292**, 912 (2001).
[7] A. T. O'Neil, I. MacVicar, L. Allen, and M. J. Padgett, Phys. Rev. Lett. **88**, 053601 (2002).
[8] R. A. Williams, J. D. Pillet, S. Al-Assam, B. Fletcher, M. Shotter, and C. J. Foot, Opt. Express **16**, 16977 (2008).
[9] P. Korda, G. C. Spalding, E. R. Dufresne, and D. G. Grier, Rev. Sci. Instrum. **73**, 1956 (2002).
[10] W. J. Hossack, E. Theofanidou, J. Crain, K. Heggarty, and M. Birch, Opt. Express **11**, 2053 (2003).
[11] J. Plewa, E. Tanner, D. M. Mueth, and D. G. Grier, Opt. Express **12**, 1978 (2004).
[12] J. E. Curtis, B. A. Koss, and D. G. Grier, Opt. Commun. **207**, 169 (2002).
[13] J. Leach, G. Sinclair, P. Jordan, J. Courtial, M. J. Padgett, J. Cooper, and Z. J. Laczik, Opt. Express **12**, 220 (2004).

[14]G. Sinclair, P. Jordan, J. Courtial, M. Padgett, J. Cooper, and Z. J. Laczik, Opt. Express **12**, 5475 (2004).
[15]A. E. Chiou, W. Wang, G. J. Sonek, J. Hong, and M. W. Berns, Opt. Commun. **133**, 7 (1997).
[16]A. Casaburi, G. Pesce, P. Zemanek, and A. Sasso, Opt. Commun. **251**, 393 (2005).
[17]E. Schonbrun, R. Piestun, P. Jordan, J. Cooper, K. D. Wulff, J. Courtial, and M. Padgett, Opt. Express **13**, 3777 (2005).
[18]E. Schonbrun, C. Rinzler, and K. B. Crozier, App. Phys. Lett. **92**, (2008).
[19]E. Schonbrun and K. B. Crozier, Opt. Lett. **33**, 2017 (2008).
[20]E. Schonbrun, A. R. Abate, P. E. Steinvurzel, D. A. Weitz, and K. B. Crozier, Lab on a Chip **10**, 852.
[21]P. Zemanek, A. Jonas, L. Sramek, and M. Liska, Opt. Commun. **151**, 273 (1998).
[22]P. Zemanek, A. Jonas, L. Sramek, and M. Liska, Opt. Lett. **24**, 1448 (1999).
[23]P. Zemanek, A. Jonas, and M. Liska, Journal of the Optical Society of America a-Optics Image Science and Vision **19**, 1025 (2002).
[24]T. Cizmar, M. Siler, M. Sery, P. Zemanek, V. Garces-Chavez, and K. Dholakia, Phys. Rev. B **74**, 035105 (2006).
[25]P. Zemanek, A. Jonas, P. Jakl, J. Jezek, M. Sery, and M. Liska, Opt. Commun. **220**, 401 (2003).
[26]W. Mu, Z. Li, L. Luan, G. C. Spalding, G. Wang, and J. B. Ketterson, J. Opt. Soc. Am. B **25**, 763 (2008).
[27]X. Y. Miao and L. Y. Lin, IEEE J. Sel. Top. Quantum Electron. **13**, 1655 (2007).
[28]M. Righini, A. S. Zelenina, C. Girard, and R. Quidant, Nature Physics **3**, 477 (2007).
[29]M. Sukharev and T. Seideman, J. Chem. Phys. **126**, 204702 (2007).
[30]L. Huang, S. J. Maerkl, and O. J. F. Martin, Opt. Express **17**, 6018 (2009).
[31]X. Y. Miao and L. Y. Lin, Opt. Lett. **32**, 295 (2007).
[32]X. Y. Miao, B. K. Wilson, S. H. Pun, and L. Y. Lin, Opt. Express **16**, 13517 (2008).
[33]M. M. Burns, J. M. Fournier, and J. A. Golovchenko, Science **249**, 749 (1990).
[34]D. Maystre and P. Vincent, Journal of Optics a-Pure and Applied Optics **8**, 1059 (2006).
[35]J. Mikhael, J. Roth, L. Helden, and C. Bechinger, Nature **454**, 501 (2008).
[36]M. P. MacDonald, G. C. Spalding, and K. Dholakia, Nature **426**, 421 (2003).
[37]R. L. Smith, G. C. Spalding, K. Dholakia, and M. P. MacDonald, Journal of Optics a-Pure and Applied Optics **9**, S134 (2007).
[38]S. C. Grover, A. G. Skirtach, R. C. Gauthier, and C. P. Grover, J. Biomed. Opt. **6**, 14 (2001).
[39]A. T. Ohta, P. Y. Chiou, T. H. Han, J. C. Liao, U. Bhardwaj, E. R. B. McCabe, F. Q. Yu, R. Sun, and M. C. Wu, J. Microelectromech. Syst. **16**, 491 (2007).
[40]J. R. Kovac and J. Voldman, Anal. Chem. **79**, 9321 (2007).
[41]L. Paterson, E. Papagiakoumou, G. Milne, V. Garces-Chavez, S. A. Tatarkova, W. Sibbett, F. J. Gunn-Moore, P. E. Bryant, A. C. Riches, and K. Dholakia, Appl. Phys. Lett. **87**, 123901 (2005).
[42]M. P. MacDonald, S. Neale, L. Paterson, A. Richies, K. Dholakia, and G. C. Spalding, Journal of Biological Regulators and Homeostatic Agents **18**, 200 (2004).
[43]P. Jakl, T. Cizmar, M. Sery, and P. Zemanek, App. Phys. Lett. **92**, 161110 (2008).
[44]K. Ladavac, K. Kasza, and D. G. Grier, Phys. Rev. E **70**, 010901 (2004).
[45]I. Ricardez-Vargas, P. Rodriguez-Montero, R. Ramos-Garcia, and K. Volke-Sepulveda, App. Phys. Lett. **88**, 121116 (2006).
[46]Y. Y. Sun, X. C. Yuan, L. S. Ong, J. Bu, S. W. Zhu, and R. Liu, App. Phys. Lett. **90**, 031107 (2007).
[47]P. T. Korda, G. C. Spalding, and D. G. Grier, Phys. Rev. B **66**, 024504 (2002).
[48]Z. P. Luo, Y. L. Sun, and K. N. An, App. Phys. Lett. **76**, 1779 (2000).
[49]K. D. Bonin, B. Kourmanov, and T. G. Walker, Opt. Express **10**, 984 (2002).
[50]U. Bockelmann, P. Thomen, B. Essevaz-Roulet, V. Viasnoff, and F. Heslot, Biophys. J. **82**, 1537 (2002).
[51]Y. Nishimura, O. Misumi, S. Matsunaga, T. Higashiyama, A. Yokota, and T. Kuroiwa, Proc. Nat. Acad. Sci. USA **96**, 12577 (1999).
[52]M. Hegner and C. Bustamante, Biophys. J. **74**, A150 (1998).
[53]M. D. Wang, H. Yin, R. Landick, J. Gelles, and S. M. Block, Biophys. J. **72**, 1335 (1997).
[54]M. D. Wang, H. Yin, R. Landick, J. Gelles, and S. M. Block, Biophys. J. **70**, SUP63 (1996).
[55]M. D. Wang, H. Yin, R. Landick, J. Gelles, and S. M. Block, Biophys. J. **70**, A44 (1996).
[56]J. M. Cruz and F. J. Garcia-Diego, Journal of Physics D-Applied Physics **31**, 1745 (1998).
[57]P. M. Hansen, V. K. Bhatia, N. Harrit, and L. Oddershede, Nano Lett. **5**, 1937 (2005).
[58]G. Gouesbet, B. Maheu, and G. Grehan, Journal of the Optical Society of America a-Optics Image Science and Vision **5**, 1427 (1988).
[59]J. P. Barton, Appl. Opt. **34**, 5542 (1995).
[60]G. Gouesbet and L. Mees, Journal of the Optical Society of America a-Optics Image Science and Vision **16**, 1333 (1999).
[61]T. Tlusty, A. Meller, and R. Bar-Ziv, Phys. Rev. Lett. **81**, 1738 (1998).
[62]B. Peterson and S. Strom, Phys. Rev. D **10**, 2670 (1974).
[63]M. I. Mishchenko, L. D. Travis, and D. W. Mackowski, Journal of Quantitative Spectroscopy & Radiative Transfer **55**, 535 (1996).
[64]B. T. Draine and P. J. Flatau, Journal of the Optical Society of America a-Optics Image Science and Vision **11**, 1491 (1994).
[65]A. Jonas, L. Sramek, M. Liska, and P. Zemanek, 11th Slovak-Czech-Polish Optical Conference on Wave and Quantum Aspects of Contemporary Optics **3820**, 70 (1999).
[66]F. Y. Cai, L. Meng, C. X. Jiang, Y. Pan, and H. R. Zheng, J. Acoust. Soc. Am. **128**, 1617 (2010).
[67]A. R. Zakharian, P. Polynkin, M. Mansuripur, and J. V. Moloney, Opt. Express **14**, 3660 (2006).
[68]A. R. Zakharian, M. Mansuripur, and J. V. Moloney, Opt. Express **13**, 2321 (2005).
[69]D. C. Benito, S. H. Simpson, and S. Hanna, Opt. Express **16**, 2942 (2008).
[70]M. Fujii, Opt. Express **18**, 27731 (2010).
[71]H. Li, S. Pan, and Y. Zhang, 5th International Symposium on Advanced Optical Manufacturing and Testing Technologies: Advanced Optical Manufacturing Technologies 7655.
[72]L. Jia and E. L. Thomas, Journal of the Optical Society of America B-Optical Physics **26**, 1882 (2009).
[73]W. S. Kim, L. Jia, and E. L. Thomas, Adv. Mater. **21**, 1921 (2009).

[74]A. Rohrbach and E. H. K. Stelzer, Journal of the Optical Society of America a-Optics Image Science and Vision **18**, 839 (2001).
[75]K. I. Petsas, A. B. Coates, and G. Grynberg, Phys. Rev. A **50**, 5173 (1994).
[76]M. Maldovan and E. L. Thomas, Applied Physics B-Lasers and Optics **83**, 595 (2006).
[77]M. Maldovan and E. L. Thomas, App. Phys. Lett. **88**, 251907 (2006).
[78]M. M. Burns, J. M. Fournier, and J. A. Golovchenko, Phys. Rev. Lett. **63**, 1233 (1989).
[79]F. J. G. de Abajo, Opt. Express **15**, 11082 (2007).
[80]J. Ng and C. T. Chan, Opt. Lett. **31**, 2583 (2006).
[81]T. M. Grzegorczyk and B. A. Kemp, Optical Trapping and Optical Micromanipulation V **7038**, S381 (2008).
[82]B. A. Kemp, T. M. Grzegorczyk, and J. A. Kong, Opt. Express **13**, 9280 (2005).
[83]B. A. Kemp, T. M. Grzegorczyk, and J. A. Kong, J. Electromagn. Waves. Appl. **20**, 827 (2006).
[84]C. K. Ullal, M. Maldovan, and E. L. Thomas, Appl. Phys. Lett. **89**, 029901 (2004).
[85]M. Wohlgemuth, N. Yufa, J. Hoffman, and L. E. Thomas, Macromolecules **34**, 6083 (2001).
[86]H. Furukawa and I. Yamaguchi, Opt. Lett. **23**, 216 (1998).
[87]A. T. O'Neil and M. J. Padgett, Opt. Commun. **185**, 139 (2000).
[88]K. Svoboda and S. M. Block, Opt. Lett. **19**, 930 (1994).
[89]Q. W. Zhan, Opt. Express **12**, 3377 (2004).
[90]J. H. Jang, C. K. Ullal, M. Maldovan, T. Gorishnyy, S. Kooi, C. Y. Koh, and E. L. Thomas, Adv. Funct. Mater. **17**, 3027 (2007).
[91]J. H. Jang, D. Dendukuri, T. A. Hatton, E. L. Thomas, and P. S. Doyle, Angewandte Chemie-International Edition **46**, 9027 (2007).
[92]P. Jiang, J. F. Bertone, and V. L. Colvin, Science **291**, 453 (2001).
[93]V. N. Manoharan, M. T. Elsesser, and D. J. Pine, Science **301**, 483 (2003).